Video Article

Epitaxial Growth of Perovskite Strontium Titanate on Germanium via Atomic Layer Deposition

Edward L. Lin[1], Bryce I. Edmondson[1], Shen Hu[1], John G. Ekerdt[1]

[1]McKetta Department of Chemical Engineering, The University of Texas at Austin

Correspondence to: John G. Ekerdt at ekerdt@utexas.edu

URL: https://www.jove.com/video/54268
DOI: doi:10.3791/54268

Keywords: Chemistry, Issue 113, Atomic layer deposition, perovskite, strontium titanate, $SrTiO_3$, germanium, epitaxy, crystalline oxide

Date Published: 7/26/2016

Citation: Lin, E.L., Edmondson, B.I., Hu, S., Ekerdt, J.G. Epitaxial Growth of Perovskite Strontium Titanate on Germanium via Atomic Layer Deposition. *J. Vis. Exp.* (113), e54268, doi:10.3791/54268 (2016).

Abstract

Atomic layer deposition (ALD) is a commercially utilized deposition method for electronic materials. ALD growth of thin films offers thickness control and conformality by taking advantage of self-limiting reactions between vapor-phase precursors and the growing film. Perovskite oxides present potential for next-generation electronic materials, but to-date have mostly been deposited by physical methods. This work outlines a method for depositing $SrTiO_3$ (STO) on germanium using ALD. Germanium has higher carrier mobilities than silicon and therefore offers an alternative semiconductor material with faster device operation. This method takes advantage of the instability of germanium's native oxide by using thermal deoxidation to clean and reconstruct the Ge (001) surface to the 2×1 structure. 2-nm thick, amorphous STO is then deposited by ALD. The STO film is annealed under ultra-high vacuum and crystallizes on the reconstructed Ge surface. Reflection high-energy electron diffraction (RHEED) is used during this annealing step to monitor the STO crystallization. The thin, crystalline layer of STO acts as a template for subsequent growth of STO that is crystalline as-grown, as confirmed by RHEED. *In situ* X-ray photoelectron spectroscopy is used to verify film stoichiometry before and after the annealing step, as well as after subsequent STO growth. This procedure provides framework for additional perovskite oxides to be deposited on semiconductors via chemical methods in addition to the integration of more sophisticated heterostructures already achievable by physical methods.

Video Link

The video component of this article can be found at https://www.jove.com/video/54268/

Introduction

Perovskite materials are becoming increasingly attractive due to their highly symmetric cubic or pseudocubic structure and myriad of properties. These materials, with general formula ABO_3, consist of A atoms coordinated with 12 oxygen atoms and B atoms coordinated with six oxygen atoms. Owing to their simple structure, yet wide range of potential elements, perovskite materials provide ideal candidates for heterostructure devices. Epitaxial oxide heterostructures boast ferromagnetic,[1-3] anti/ferroelectric,[4] multiferroic,[5-8] superconductive,[7-12] and magnetoresistive functionalities.[13,14] Many of these desirable electronic properties are interfacial and thus dependent on clean, abrupt transitions between materials. The nearly identical structure and lattice constants shared between members of the perovskite family allow for excellent lattice matching and, therefore, high quality interfaces. Readily lattice-matched to each other as well as some semiconductors, perovskite oxides are now being turned to in next generation metal-oxide-semiconductor electronics.

Monolithic integration of crystalline oxides with silicon, first demonstrated with perovskite strontium titanate, $SrTiO_3$ (STO), by McKee and colleagues,[15] was a monumental step towards the realization of electronic devices with perovskite-semiconductor incorporation. Molecular beam epitaxy (MBE) is the primary technique for epitaxial growth of oxides on silicon because of the layer-by-layer growth as well as the tunable oxygen partial pressure necessary to control amorphous, interfacial SiO_2 formation.[16-19] Typical MBE growth of STO on Si (001) is achieved by Sr-assisted deoxidation of SiO_2. Under the ultra-high vacuum (UHV) conditions, SrO is volatile and subject to thermal evaporation. Since SrO is thermodynamically preferred over strontium metal and SiO_2, deposition of Sr scavenges oxygen from the SiO_2 layer and the resulting SrO evaporates from the surface. During this process the silicon surface experiences a 2×1 reconstruction at the surface that forms rows of dimerized silicon atoms. Conveniently, ½ monolayer (ML) coverage of Sr atoms on the reconstructed surface fills in the gaps created by these dimer rows.[20] The ½ ML coverage provides a protective layer that, with careful control of oxygen pressure, can prevent or control interfacial SiO_2 formation during subsequent oxide growth.[21-23] In the case of STO (and perovskites with similar lattice match), the resulting lattice is rotated 45° in-plane such that $(001)_{STO}\|(001)_{Si}$ and $(100)_{STO}\|(110)_{Si}$, allowing registry between the Si (3.84 Å Si-Si distance) and STO (a = 3.905 Å) with only slight compressive strain on the STO. This registry is necessary for high quality interfaces and the desired properties they possess.

Silicon became industrially significant due to the high quality of its interfacial oxide, but SiO_2 use is being phased out for materials capable of equivalent performance at smaller feature sizes. SiO_2 experiences high leakage currents when ultra-thin and this diminishes device performance. The demand for smaller feature sizes could be met by perovskite oxide films with high dielectric constants, k, that provide performance equivalent to SiO_2 and are physically thicker than SiO_2 by the factor k/3.9. Furthermore, alternative semiconductors, like germanium, offer potential for faster device operation due to higher electron and hole mobilities than silicon.[24,25] Germanium also has an interfacial oxide, GeO_2,

but in contrast to SiO_2, it is unstable and subject to thermal deoxidation. Thus, 2×1 reconstruction is achievable by simple thermal annealing under UHV, and a protective Sr layer is unnecessary to prevent interfacial oxide growth during perovskite deposition.[26]

Despite the apparent ease of growth offered by MBE, atomic layer deposition (ALD) provides a more scalable and cost effective method than MBE for the commercial production of oxide materials.[27,28] ALD employs doses of gaseous precursors to the substrate that are self-limiting in their reaction with the substrate surface. Therefore, in an ideal ALD process, up to one atomic layer is deposited for any given precursor dosing cycle and continued dosing of the same precursor will not deposit additional material onto the surface. Reactive functionality is restored with a co-reactant, often an oxidative or reductive precursor (*e.g.*, water or ammonia). Previous work has demonstrated the ALD growth of various perovskite films, such as anatase TiO_2, $SrTiO_3$, $BaTiO_3$, and $LaAlO_3$, on Si (001) that had been buffered with four-unit-cell thick STO grown via MBE.[29-34] In purely MBE growth of crystalline oxides, ½ monolayer coverage of Sr on clean Si (001) is enough to provide a barrier against SiO_2 formation under the pressures native to the technique (~10^{-7} Torr). However, under typical ALD operating pressures of ~1 Torr, previous work has shown that four unit cells of STO is required to avoid oxidizing the Si surface.[29]

The procedure detailed here utilizes the instability of GeO_2 and achieves monolithic integration of STO on germanium via ALD without the need of an MBE-grown buffer layer.[26] Furthermore, the Ge-Ge interatomic distance (3.992 Å) on its (100) surface allows for an analogous epitaxial registry with STO that is observed with Si (001). Though the procedure presented here is specific to STO on Ge, slight modifications may allow for the monolithic integration of a variety of perovskite films on germanium. Indeed, direct ALD growth of crystalline $SrHfO_3$ and $BaTiO_3$ films have been reported on Ge.[35,36] Additional possibilities include the potential gate oxide, $SrZr_xTi_{1-x}O_3$.[37] Finally, building on previous studies of ALD perovskite growth on a four-unit cell STO film on Si (001)[29-34] suggests that any film that could be grown on the STO/Si platform could be grown on an ALD-grown STO buffer film on Ge, such as $LaAlO_3$ and $LaCoO_3$.[32,38] The multitude of properties available to oxide heterostructures and remarkable similarity between perovskite oxides suggest this procedure could be utilized to study previously difficult or impossible growth combinations with such an industrially viable technique.

Figure 1 depicts the schematic of the vacuum system, which encompasses ALD, MBE, and analytical chambers connected by a 12-foot transfer line. The samples can be transferred *in vacuo* between each chamber. The baseline pressure of the transfer line is kept at approximately 1.0×10^{-9} Torr by three ion pumps. The commercial angle-resolved ultraviolet and X-ray photoelectron spectroscopy (XPS) system is maintained with an ion pump such that the pressure in the analytical chamber is kept at approximately 1.0×10^{-9} Torr.

The ALD reactor is a rectangular custom-built stainless steel chamber with a volume of 460 cm^3 and length of 20 cm. A schematic of the ALD reactor is shown in **Figure 2**. The reactor is a hot wall, continuous cross-flow type reactor. Samples placed in the reactor have a clearance of 1.7 cm between the top surface of the substrate and the chamber ceiling and 1.9 cm between the bottom of the substrate and the chamber floor. A heating tape, powered by a dedicated power supply, is wrapped around the chamber from the inlet to approximately 2 cm beyond the exhaust port and provides temperature control of the reactor walls. A temperature controller adjusts the power input to the heating tape according to a temperature measurement taken by a thermal couple located between the heating tape and exterior reactor wall. The reactor is then completely wrapped with three additional heating tapes of constant power provided by a variac, and a final layer of fiberglass wool with aluminum foil covering provides insulation to promote uniform heating. The power output of the variac is adjusted such that the idling temperature (when the dedicated power supply is turned off) of the reactor is approximately 175 °C. The reactor is passively cooled via ambient air. The substrate temperature is calculated using the linear-fit equation (1), where T_s (°C) is the temperature of substrate and T_c (°C) is the temperature of the reactor wall, obtained by directly measuring a substrate fitted with a thermocouple. A temperature profile exists along the flow direction of the chamber due to the cold gate valve that connects the reactor to the transfer line; the temperature profile perpendicular to the flow direction is negligible. The temperature profile causes a richer Sr deposition at the leading edge of the sample, but the composition variation along sample is small (less than a 5% difference between the leading and trailing edges of the sample) according to XPS.[31] The exhaust of the reactor is connected to a turbomolecular pump and a mechanical pump. During the ALD process, the reactor is pumped by the mechanical pump to maintain the pressure at around 1 Torr. Otherwise, the reactor pressure is maintained below 2.0×10^{-6} Torr by the turbomolecular pump.

(1) $T_s=0.977T_c + 3.4$

The MBE chamber is maintained at a baseline pressure of approximately 2.0×10^{-9} Torr or below by a cryogenic pump. The partial pressure of various species in the MBE chamber is monitored by a residual gas analyzer. The background pressure of H_2 is around 1.0×10^{-9} Torr, while those of O_2, CO, N_2, CO_2, and H_2O, are less than 1.0×10^{-10} Torr. In addition, the MBE chamber is also equipped with six effusion cells, a four-pocket electron beam evaporator, an atomic nitrogen plasma source and an atomic oxygen plasma source with high-precision piezoelectric leak valve, and a reflection high energy electron diffraction (RHEED) system for real-time *in situ* growth and crystallization observations. The sample manipulator allows the substrate be heated up to 1000 °C using an oxygen-resistant silicon carbide heater.

Protocol

1. Preparing Sr and Ti Precursors for ALD Experiments

1. Load the clean, dry saturators and new precursors into the antechamber of a glove box. Follow the glove box's loading procedure to ensure proper purging of air and moisture. Transfer the materials into the main chamber.
   Note: This group uses in-house built saturators (see **Figure 3**) with components purchased commercially. Details of the saturator assembly can be found in the List of Specific Reagents and Equipment.
2. Store the strontium precursor (strontium bis(triisopropylcyclopentadienyl) [$Sr(^iPr_3Cp)_2$]) and titanium precursor (titanium tetraisopropoxide [$Ti(O\text{-}^iPr)_4$], TTIP) in an inert environment (*e.g.*, a glove box) after opening the original packaging provided by the manufacturer.
   Note: This group uses a glovebox with a moisture level no greater than 5 ppm.
3. Load the precursor into the saturator such that the precursor occupies approximately 2/3 of the glass part of the saturator (about 5 g).
4. Reassemble the saturators and ensure a good leak tight seal is achieved.
   Note: This group uses metal gasket face seal fittings to achieve leak tight seals.
5. Unload the filled saturators from the glove box and connect the filled saturators to the ALD manifold.

Note: The loaded precursors can be used multiple times over an extended period. The precursors in this group's system generally require refilling every six months as they become consumed. $Sr(^{i}Pr_3Cp)_2$ is a brown liquid at both RT and the operating temperature for this study (130 - 140 °C). TTIP is a clear liquid. When TTIP deteriorates, typically due to moisture and/or air contamination, the precursor will turn into a white solid. There has been no visible indicator of precursor deterioration for the $Sr(^{i}Pr_3Cp)_2$ observed by this group. Sr precursor deterioration is generally detected by a significant decrease (greater than 10%) of Sr content in a repeatable ALD growth that utilizes $Sr(^{i}Pr_3Cp)_2$.

2. Cleaning the Ge (001) Substrate

1. Place a Ge (001) substrate (18 mm × 20 mm), polished side facing upwards, into a small beaker (25-50 ml). Fill the beaker to about 1 cm height with acetone. Place the beaker in a bath sonicator and sonicate for 10 min.
   Note: This group uses single-side polished 4-in Ge wafers, cut into 18 × 20 mm^2 pieces using a dicing saw. Use heavily doped n-type Ge if electrical measurements of the film are needed (this study uses Sb-doped Ge wafers with ρ ≈ 0.04 Ω-cm), otherwise all doping level and dopant types are acceptable.
2. Decant the majority of the acetone into a waste container, taking care not to pour out or flip the Ge substrate. Rinse the walls of the beaker with isopropyl alcohol (IPA) and fill to approximately 1 cm height. Pour the majority of the IPA into a waste container, refill beaker to 1 cm with IPA, and sonicate for another 10 min.
3. Repeat step 2.2, but replace IPA with deionized water.
4. Remove the substrate from the beaker with tweezers. Dry the substrate with a nitrogen gun or other dry inert gas flow.
5. Place the substrate in the UV-ozone cleaner and run the cleaner for 30 min.
6. After UV-ozone cleaning, immediately load the substrate into the vacuum system.

3. Loading the Ge Substrate

1. Move the transfer line sample carrier-cart into the load lock. Close the gate-valve to isolate the load lock.
2. Turn off the load lock turbomolecular pump and open the nitrogen line to vent the load lock. Complete Step 3.3 while waiting for the load lock to completely vent.
3. Place the substrate, polished side facing downward, into a 20 mm × 20 mm sample holder.
   Note: All depositions are performed with the sample facing downward. Ensure the substrate is flush with the bottom of the holder; otherwise RHEED experiments may experience difficulty and films may not deposit uniformly. A sample holder this group uses is shown in **Figure 4**.
4. Open the load lock after it has completely vented. Place the sample holder into an open carrier-cart position by aligning the tabs of the sample holder with the channels of the open cart position and lowering it into place.
5. Close the load lock and turn on the load lock turbomolecular pump. Close the nitrogen line.
6. Wait until the pressure in the load lock is approximately 5.0×10^{-7} Torr before opening the load lock gate valve and moving the cart through the transfer line.

4. Ge Deoxidization

1. Transfer the Ge substrate into the MBE chamber.
2. Ramp the Ge substrate temperature to 550 °C at 20 °C•min^{-1} and then to 700 °C at 10 °C•min^{-1}. After holding the sample at 700 °C for 1 hr, cool the sample to 200 °C with a 30 °C•min^{-1} ramp rate.
3. Use RHEED to confirm the 2×1 reconstructed surface as described in Representative Results section.[26,39]
4. Optional: Use XPS to ensure that the Ge (001) substrate is free of oxides (described in Section 8).

5. Thin Film ALD Growth of STO on Ge Substrate

1. Adjust the ALD reactor temperature to 225 ºC.
2. Heat $Sr(^{i}Pr_3Cp)_2$ to 130 °C and TTIP to 40 °C. Maintain water at RT (between 20 and 25 °C). Regulate the water vapor flow into the ALD system *via* the needle valve attached to the saturator such that the dosing pressure of water is around 1 Torr. Maintain constant precursor temperatures throughout the deposition process.
3. Transfer the sample *in vacuo* to the ALD reactor that has been preheated to 225 °C and wait for 15 min for the sample to reach thermal equilibrium.
4. Switch the exhaust port of the ALD reactor from the turbomolecular pump to the mechanical pump.
5. Turn on the flow controller to allow the flow of inert gas (this group uses argon). Maintain an operating pressure of 1 Torr during the entire growth process.
6. Set the unit cycle ratio of Sr to Ti to be 2:1. Set the unit cycles of Sr and Ti to a 2-sec dose of the Sr or Ti precursor, followed by a 15-sec argon purge, and then a 1-sec dose of water, followed by another 15-sec argon purge.
7. Adjust the number of unit cycles to achieve the desirable thickness. Ensure that the ALD cycling sequence contains as little repetition of individual Sr or Ti unit cycles as possible. For example, a 2:3 Sr-to-Ti cycling sequence will achieve better results when executed as 1-Sr, 1-Ti, followed by 1-Sr, 2-Ti, rather than 2-Sr followed by 3-Ti.
   Note: This group used 36 unit cycles to deposit a 2-nm thick STO film on Ge.
8. Optional: Use XPS to verify the film composition (described in Section 8).

6. Annealing of STO Film

1. Transfer the deposited sample *in vacuo* into the annealing chamber.

2. Heat the sample to 650 °C at a rate of 20 °C•min^{-1} under UHV conditions (10^{-9}- 10^{-8} Torr). Hold the temperature at 650 ºC for 5 min, and then cool the sample to 200 °C at the same rate.
Note: Use RHEED to evaluate the annealing result, as described in the Representative Results section.[26,39]

7. Further Growth of STO

1. Repeat Section 5.1 - 5.5.
2. Set the unit cycle ratio to between 1:1 and 4:3. Maintain the same dosing/purging component within each unit cycle. Set the sequence according to the principles mentioned in Step 5.6.
3. Adjust the number of unit cycles to achieve the intended thickness.
4. Anneal the deposited film according to Section 6 of the Protocol.

8. XPS Measurements

1. Load the sample into the XPS analytical chamber and turn on the X-ray source. Ensure all appropriate gates/doors are closed to prevent accidental X-ray exposure.
2. Create a new scan by selecting the elements (binding energy ranges) desired for analysis, or select a pre-existing scan program.
Note: Binding energy ranges can be manually changed, if needed. Set other settings, such as pass energy, excitation energy, step energy, and step time to optimize the signal-to-noise ratio, but remain constant across all elemental scans to maintain comparability between elemental spectra. **Table 1** shows the scan settings used by this group.
3. Check if any charging is occurring on the substrate by observing the binding energy of a known element's peak, such as O *1s* at 531 eV.
Note: Charging is occurring if the peak has shifted from its known value.
4. Insert a flood gun into the XPS chamber and turn on the flood gun if charging is occurring. Adjust the flood gun energy output and distance from the sample so that the chosen peak is shifted back to its correct binding energy.
5. Manipulate the stage position to maximize the area observed under a known element's peak (typically the O 1*s* peak at 531 eV).
6. Run the XPS scan and collect the data.
7. Turn off the X-ray source and remove the sample from the XPS.

Representative Results

Figures 5 and **6** show typical X-ray photoelectron spectra and RHEED images from a cleaned and deoxidized Ge substrate. A successfully-deoxidized Ge substrate is characterized by its "smiley face" 2×1 reconstructed RHEED pattern.[26,39] In addition, Kikuchi lines are also observed in the RHEED images, which indicate the cleanliness and long range order of the sample.[40] The sharpness and intensity of the diffraction pattern also demonstrate the cleanliness of the surface. The Ge 3*d* X-ray photoelectron spectrum should be free of oxidized Ge peaks, with the Ge^0 peak observed at 30 eV. This can also be confirmed by the absence of an O 1*s* feature at 531 eV.

The ALD-grown STO film is amorphous upon deposition and exemplified via a hazy RHEED image, such as that of **Figure 6B**. In order to achieve a crystalline film upon annealing, the ALD parameters are adjusted such that a slightly Sr-rich stoichiometry is obtained in the deposited STO film. This group typically aims for a ratio between Sr to total Sr and Ti (*i.e.*, Sr/(Sr+Ti)) of 0.53 - 0.54. The film composition can be verified *via* integration of the X-ray photoelectron spectra with appropriate relative sensitivity factors and other parameters as shown in Section 8 of the Protocol. This group obtained the parameters by both consulting the *Handbook of X-ray Photoelectron Spectroscopy* by Moulder *et al.*,[41] as well as using commercially available perovskite crystals as standards. A poor stoichiometric ratio between Sr and Ti (*i.e.*, when the film is Ti-rich or Sr/(Sr+Ti) is greater than 0.57) will result in poor crystallinity, or even the lack thereof, after the annealing step.

Once the STO film has been annealed, its crystallinity can be observed *via* the RHEED pattern, as shown in **Figures 6C** and **6D**. The RHEED pattern of an STO film with good epitaxial growth on Ge should exhibit sharp streak patterns. The crystallinity of the deposited STO film can also be confirmed by X-ray diffraction. **Figure 7** depicts the X-ray diffraction pattern of epitaxial STO on Ge with characteristic peaks of STO (001) at 22.8°, STO (002) at 46.5°, and Ge (004) at 66.0°. The epitaxial nature of the film can be directly confirmed by cross-sectional high-resolution transmission electron microscopy (HRTEM). **Figure 8** shows the high quality epitaxial registry between STO and Ge as well as the abrupt transition between layers.

Electrical measurements of epitaxial STO on Ge can also be conducted. **Figure 9** shows the capacitance-voltage (CV) and current-voltage (IV) measurements of a metal-insulator-semiconductor (MOS) capacitor created by depositing a 50-µm radius Ti/Au top electrode on STO/n +Ge (001). The CV measurement of a 15-nm STO film from **Figure 9A** suggests the capacitance of the structure is 5.3 µF/cm^2. The dielectric constant of the STO film is therefore approximately 90 and yields an equivalent oxide thickness less than 0.7 nm. **Figure 9B** shows the leakage current density of the MOS capacitor is approximately 10 A/cm^2 at an applied field of 0.7MV/cm. The high leakage current density should be expected due to the lack of conduction band offset between STO and Ge. Depositing other films on Ge, such as Al-doped STO and strontium hafnate (SHO), improves the leakage current density.[26,35] In fact, SHO gives a leakage current density of less than 10^{-5} A/cm^2 at the same applied field.

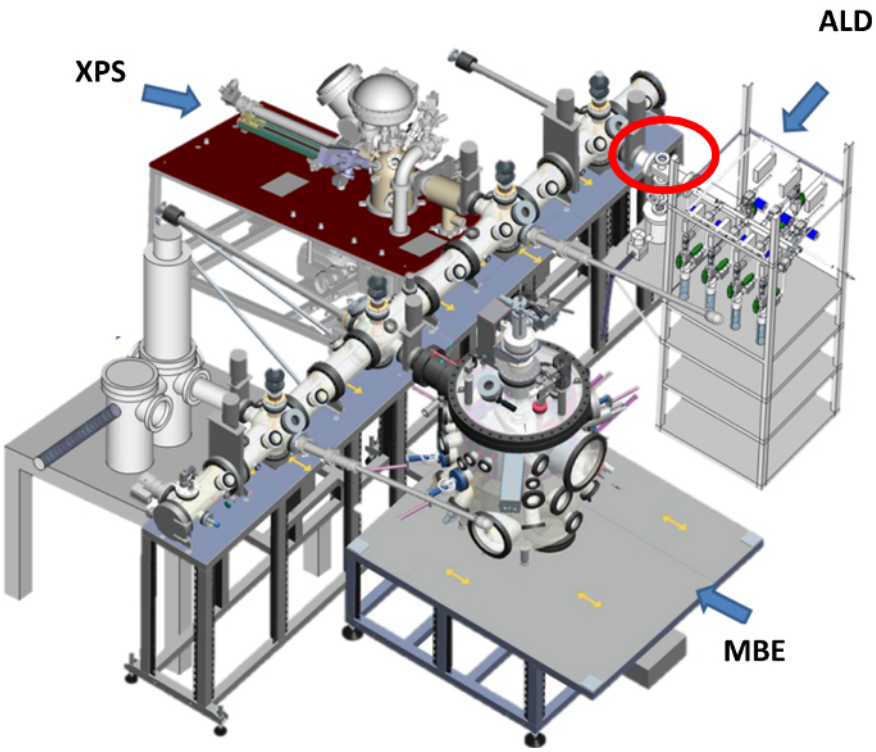

Figure 1. Schematic of the connected vacuum system. The vacuum system contains MBE, ALD, and analytical chambers connected together by an ultra-high vacuum transfer line, allowing *in vacuo* sample transfer. Please click here to view a larger version of this figure.

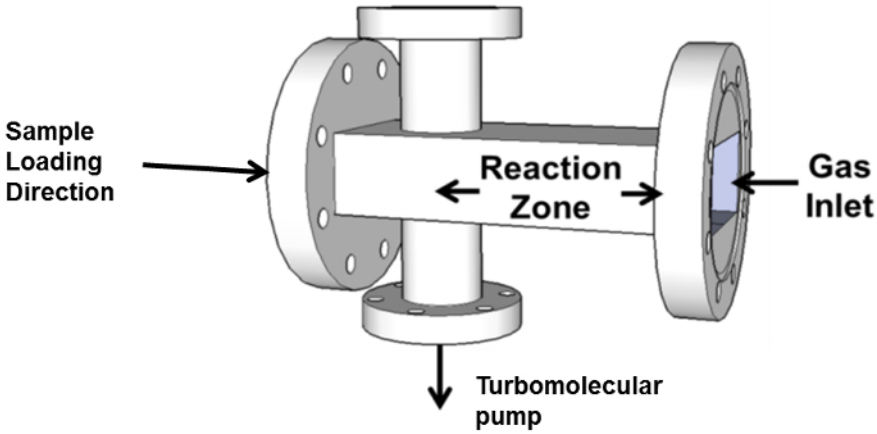

Figure 2. ALD reactor design. The ALD chamber has a volume of 460 cm^3 and length of 20 cm. The carrier gas delivers precursors from the saturators to the reactor, and exhaust gases are removed through the turbomolecular pump port. The sample is transferred to the reaction zone from the reactor end opposite to the gas inlet. Please click here to view a larger version of this figure.

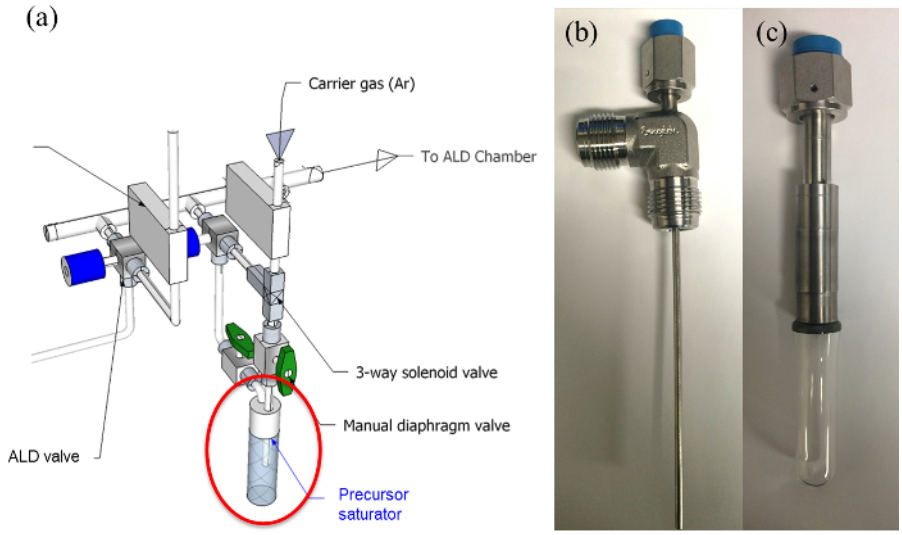

Figure 3. ALD precursor saturator. (**A**) Schematic of this group's custom built saturator as well as other parts used for precursor delivery into the ALD chamber. (**B**) and (**C**) show the top and bottom part of the saturator, respectively. The two parts are connected *via* a VCR fitting, and are disassembled when filling the saturator. All parts are made of 316 stainless steel, with the exception of a Pyrex-to-stainless steel adaptor, and are connected together *via* butt welding. Detailed information of these parts can be found in the List of Specific Reagents and Equipment. Please click here to view a larger version of this figure.

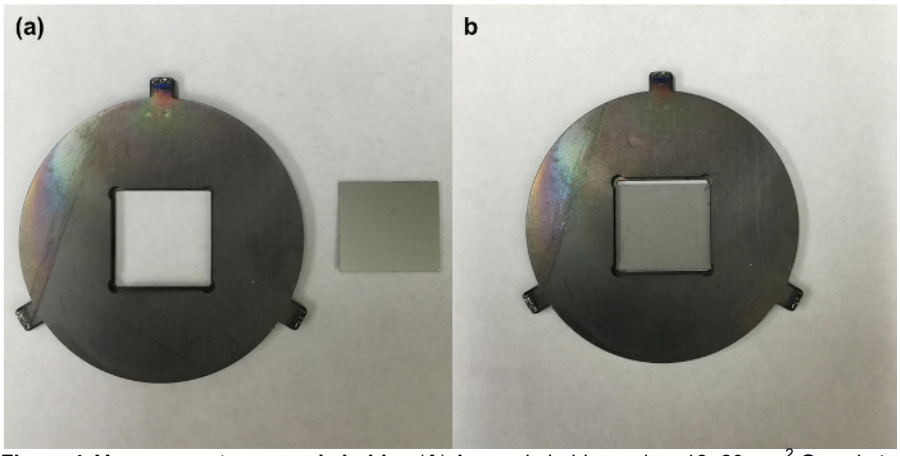

Figure 4. Vacuum system sample holder. (**A**) A sample holder and an 18×20 mm^2 Ge substrate. (**B**) A sample holder with the Ge substrate loaded. Note that the polished side is facing down. Please click here to view a larger version of this figure.

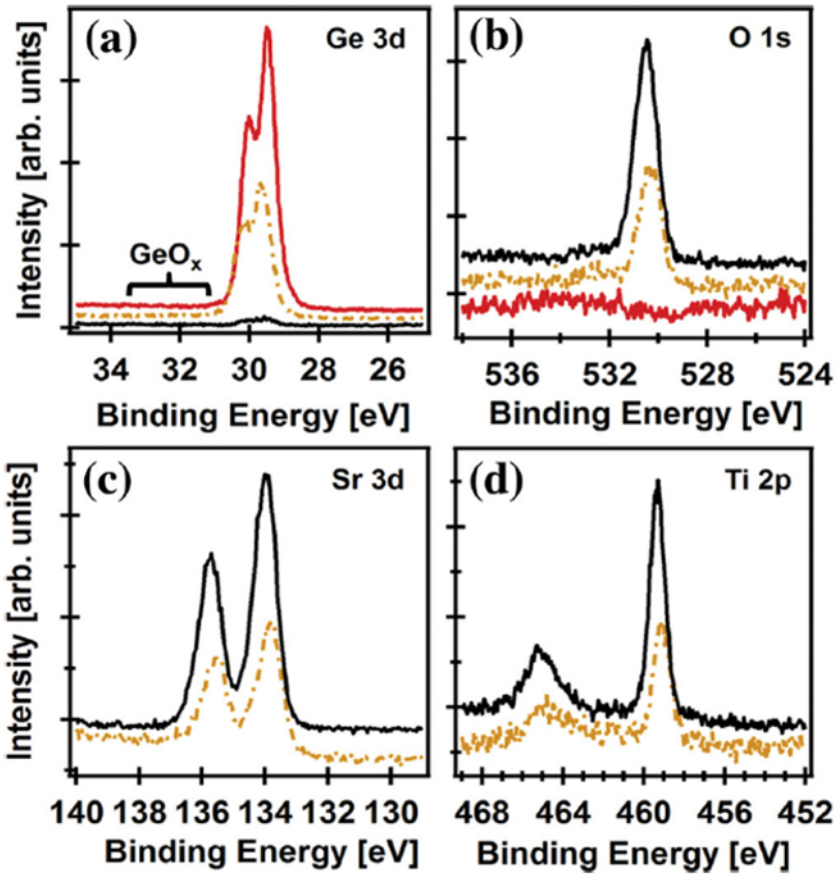

Figure 5. X-ray photoelectron spectra. (**A**) Ge 3*d,* (**B**) O 1*s,* (**C**) Sr 3*d*, and (**D**) Ti 2*p* before ALD growth (solid red line), after 36 unit cycles (~2 nm STO) (dashed brown line), and after 155 unit cycles (~8 nm STO) (solid black line). Please click here to view a larger version of this figure.

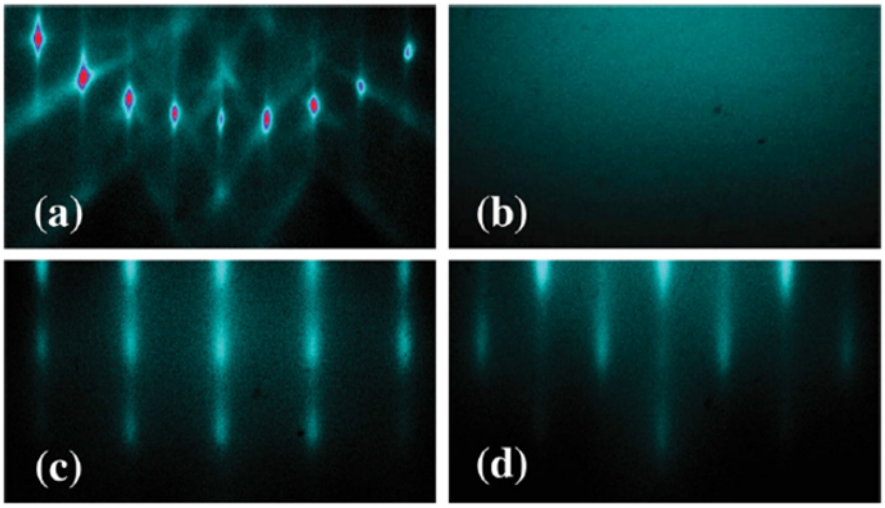

Figure 6. RHEED images. (**A**) A clean Ge substrate after thermal deoxidation, (**B**) after the second STO deposition (155 unit cycles, as-deposited), and (**C**)-(**D**) after annealing at 650 °C. The beam is aligned along the [110] and [100] azimuth for (**C**) and (**D**), respectively. Please click here to view a larger version of this figure.

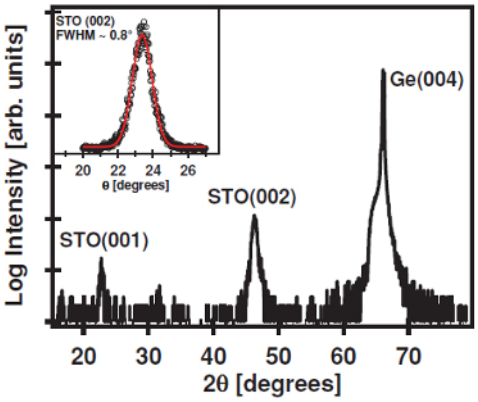

Figure 7. X-ray diffraction pattern. The diffraction pattern for a 15-nm thick STO film grown by ALD on Ge (001) at 225 °C. Inset: rocking curve around the STO (002) peak. Please click here to view a larger version of this figure.

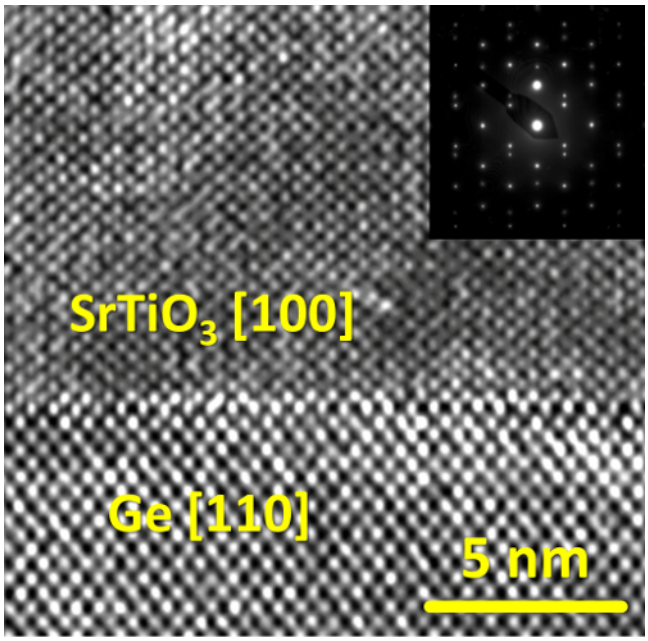

Figure 8. Cross-sectional high-resolution transmission electron micrograph. HRTEM depicts high quality STO on Ge. Inset: selected-area electron diffraction pattern showing epitaxial registry between the substrate and film. Please click here to view a larger version of this figure.

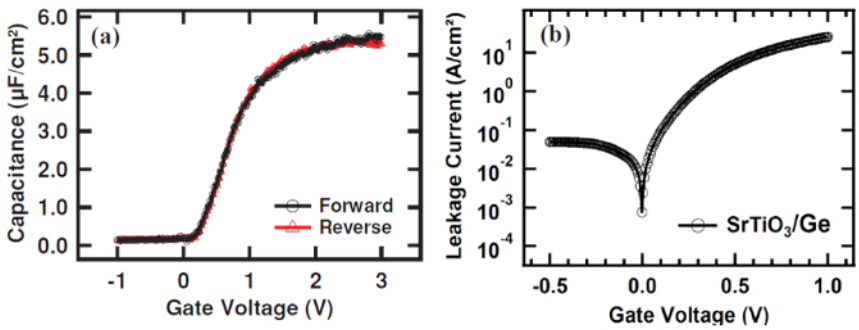

Figure 9. C-V and I-V curve of a MOS capacitor with STO. (**A**) Specific capacitance as a function of voltage bias for a 15-nm thick STO film on n+ Ge (001) by ALD, and (**B**) the gate leakage current density as a function of voltage bias measured from a typical Au(Ti)/STO/Ge structure. The metal-insulator-semiconductor capacitor structure was created by depositing 50-μm radius Ti/Au top electrode on the STO film. Please click here to view a larger version of this figure.

Region Name	Lens Mode	Pass Energy (eV)	Excitation Energy (eV)	Energy Mode	Energy (eV)		Energy Step (meV)	Step Time (sec)	Steps
					Low	High			
Survey Scan	Transmission	200	1486.6	Binding	0	1300	800	0.286	1657
Sr 3d	Transmission	100	1486.6	Binding	127.805	140.1942	50	0.157	499
Ti 2p	Transmission	100	1486.6	Binding	449	471	50	0.157	691
O 1s	Transmission	100	1486.6	Binding	515	545	50	0.157	851
C 1s	Transmission	100	1486.6	Binding	277.5	302.5	50	0.157	751
Ge 3d	Transmission	100	1486.6	Binding	24	36	50	0.157	491

Table 1. XPS Scan Settings.

Discussion

The cleanliness of the Ge substrate is the key to success when growing the epitaxial perovskite using ALD. The amount of time a Ge substrate spends between degreasing and deoxidization, and the amount of time between deoxidization and STO deposition, should be kept at a minimum. Samples are still subject to contaminant exposure even under the UHV environment. Prolonged exposure may lead to redeposition of adventitious carbon or Ge reoxidation, resulting in poor film growth. This group has employed a widely-used degreasing procedure (sonication in acetone/IPA/DI-water with subsequent UV-ozone exposure) to remove the carbon contaminants. Another procedure using oxygen plasma under UHV conditions can also be used to remove carbon contaminants.[39] The oxygen plasma will also oxidize the surface of the Ge substrate, but the oxide can be removed in a subsequent Ge deoxidization protocol. The thermal deoxidation of the GeO_2 protocol presented here is effective for the purposes of the perovskite growth in this study.

In addition to the cleanliness of the substrate, it is imperative to achieve the slightly Sr-rich stoichiometry, ideally between 0.53 and 0.54 Sr/(Sr+Ti), in order to achieve crystallization during the annealing step. While films with Sr/(Sr+Ti) of between 0.48 and 0.57 can all crystallize to various extents, this group has experimentally found that STO films with Sr/(Sr+Ti) between 0.53 and 0.54 crystallize most easily. That is, onset crystallization can be observed at a lower temperature during temperature ramping (Step 6.2) than films with other compositions. The stoichiometry between Sr and Ti is determined by various parameters of the deposition process, such as precursor temperature, dosing and purging time, substrate temperature, and unit cycle ratio. The selection of these parameters largely depends on the reaction kinetics of each ALD precursor. Enough precursor vapor pressure is needed in the reactor chamber to drive the equilibrium toward complete surface coverage and adsorption of precursor molecules. A suitable precursor temperature and dosing time will ensure a precursor saturates the substrate surface during the dosing step of an ALD unit cycle. The precursor temperature employed in an ALD experiment is determined by reviewing a combination of reports in the literature, manufacturers' specifications, and previous experimental experience with the compounds. This group typically adjusts the precursor temperature such that the precursor vapor pressure is approximately 0.1 Torr. Due to the variation between different deposition system designs, some trial-and-error is generally needed to find the precursor temperature when adopting a new precursor. Similarly, sufficient purging time is required such that the ALD chamber is free of the previously-dosed precursor molecules. This ensures a true ALD process-depositing one material at a time rather than a CVD-like continuous deposition. ALD precursors also possess temperature windows (the "ALD window") where the deposition rate will be nearly independent of the substrate temperature. During deposition the precursor molecules will saturate the substrate surface, preventing additional molecules from adsorbing onto the surface. As a result, the amount of molecules-and atoms-deposited every cycle will be limited by the reactant adsorption properties and kinetics. For a ternary oxide like STO, the two precursors may still have different rates of deposition. Hence, the unit cycle ratio between the precursors needs to be established experimentally. This group has settled on the parameters mentioned in Sections 5 to 7 in the Protocol section *via* product specifications from manufacturers, reports from literature,[42-45] and data from past experiments.[29,30]

It was found through experiments that even though Sr:Ti cycle ratios of near 1:1 yielded stoichiometric STO films on STO-buffered Si (001), a 2:1 Sr:Ti cycle ratio is needed for the initial STO growth on Ge.[26] As a result, a two-step ALD growth is used for STO films thicker than 2 nm. The STO films deposited using Steps 5 to 7 of the Protocol will be amorphous as-deposited and it is necessary to anneal the films. The annealing temperature is established experimentally.[26,29,30,] The need for annealing temperatures higher than 650 °C may indicate problems with the substrate, such as an incompletely cleaned substrate surface or stoichiometry deviating from ideal to slightly Sr-rich stoichiometry (*e.g.*, ideal $SrTiO_3$ has 20, 20, and 60 atomic% of Sr, Ti, and O, respectively). Although the theoretical perovskite stoichiometry should yield the best possible crystallinity, slightly A-rich films were observed to crystallize better than stoichiometric or B-rich films. If the ratio of Sr/(Sr+Ti) is beyond the range of 0.48 to 0.57, it will be hard to crystallize the film during the annealing process. This group has annealed STO films in the MBE chamber equipped with *in situ* RHEED to monitor the process of crystallization, and thus decided the parameters for the annealing procedure.

After the completion of Sections 4, 5, 6, and 7 of the Protocol, one will have the option of evaluating the sample *via* XPS. This group used *in situ* XPS for all the XPS measurements discussed in this article, *i.e.*, the samples remained in the UHV system at all times. The use of *in situ* XPS allows for accurate evaluation of the result after each step of the experiment. Therefore, the carbon content-a common contaminant in ALD-in the deposited film can be evaluated without concerns for contamination from ambient carbon sources. The samples were also not exposed to an oxidative atmosphere after growth, which eliminates the possibility of altering film properties *via* oxidation.

Although the stoichiometric ratio between Sr and Ti in the deposited STO film can be adjusted by manipulating the unit cycle ratio, the stoichiometric ratio may not vary linearly with respect to the ratio between the two precursors. STO films, among other perovskites, are more tolerant toward Ti deficiency (B-site vacancies of the perovskite) as opposed to that of Sr (A-site).[26,31,33] A good stoichiometry (between 0.53 and 0.54 Sr/(Sr+Ti)) will result in a lower crystallization temperature during annealing. Using the prescribed protocol, this group has grown stoichiometric, crystalline STO films of up to 15 nm in thickness.[26] To grow a thicker film, one might need to deposit the film in multiple growth-and-anneal steps, or try to promote *in situ* crystallization. With a higher deposition temperature, the film may crystallize upon deposition. A

drawback of promoting *in situ* crystallization is that the roughness of the films seems to be greater than those films crystallized by annealing an amorphous film after deposition.[46]

The ALD of STO on Ge experiment discussed in this article may be easily modified to deposit A-site and B-site substituted perovskite films. This can be done by substituting some of the Sr or Ti unit cycles with those of desirable elements, such as lanthanum for the A-site and hafnium for the B-site. It is also possible to apply the principles behind this protocol when growing other ABO_3 perovskite films, such as strontium hafnate (SHO)[35] and barium titanate (BTO),[36] epitaxially on Ge (001). The various properties of lattice-matched perovskite oxides provide will enable the development of monolithically integrated perovskite-based microelectronic devices. This work has demonstrated the potential of growing crystalline oxides for the application of advanced electronic applications in the near future, especially for high-mobility semiconductor materials such as Ge.

Disclosures

The authors have no competing financial interests to disclose.

Acknowledgements

This research was supported by the National Science Foundation (Awards CMMI-1437050 and DMR-1207342), the Office of Naval Research (Grant N00014-10-10489), and the Air Force Office of Scientific Research (Grant FA9550-14-1-0090).

References

1. Phan, M.-H., & Yu, S.-C. Review of the magnetocaloric effect in manganite materials. *J. Magn. Magn. Mater.* **308** (2), 325-340 (2007).
2. Serrate, D., Teresa, J. M. D., & Ibarra, M. R. Double perovskites with ferromagnetism above room temperature. *J. Phys. Condens. Matter.* **19** (2), 023201 (2007).
3. Cheng, J.-G., Zhou, J.-S., Goodenough, J. B., & Jin, C.-Q. Critical behavior of ferromagnetic perovskite ruthenates. *Phys. Rev. B.* **85** (18), 184430 (2012).
4. Ahn, C. H. Ferroelectricity at the Nanoscale: Local Polarization in Oxide Thin Films and Heterostructures. *Science.* **303** (5657), 488-491 (2004).
5. Catalan, G., & Scott, J. F. Physics and Applications of Bismuth Ferrite. *Adv. Mater.* **21** (24), 2463-2485 (2009).
6. Ramesh, R., & Spaldin, N. A. Multiferroics: progress and prospects in thin films. *Nat. Mater.* **6** (1), 21-29 (2007).
7. Vrejoiu, I., Alexe, M., Hesse, D., & Gösele, U. Functional Perovskites - From Epitaxial Films to Nanostructured Arrays. *Adv. Funct. Mater.* **18** (24), 3892-3906 (2008).
8. Jang, H. W., *et al.* Metallic and Insulating Oxide Interfaces Controlled by Electronic Correlations. *Science.* **331** (6019), 886-889 (2011).
9. Hwang, H. Y., *et al.* Emergent phenomena at oxide interfaces. *Nat. Mater.* **11** (2), 103-113 (2012).
10. Stemmer, S., & Millis, A. J. Quantum confinement in oxide quantum wells. *MRS Bull.* **38** (12), 1032-1039 (2013).
11. Stemmer, S., & James Allen, S. Two-Dimensional Electron Gases at Complex Oxide Interfaces. *Annu. Rev. Mater. Res.* **44** (1), 151-171 (2014).
12. Biscaras, J., *et al.* Two-dimensional superconductivity at a Mott insulator/band insulator interface $LaTiO_3/SrTiO_3$. *Nat. Commun.* **1**, 89 (2010).
13. Dagotto, E. Complexity in Strongly Correlated Electronic Systems. *Science.* **309** (5732), 257-262 (2005).
14. Jin, K., *et al.* Novel Multifunctional Properties Induced by Interface Effects in Perovskite Oxide Heterostructures. *Adv. Mater.* **21** (45), 4636-4640 (2009).
15. McKee, R. A., Walker, F. J., & Chisholm, M. F. Crystalline oxides on silicon: the first five monolayers. *Phys. Rev. Lett.* **81** (14), 3014 (1998).
16. Warusawithana, M. P., *et al.* A Ferroelectric Oxide Made Directly on Silicon. *Science.* **324** (5925), 367-370 (2009).
17. Niu, G., Vilquin, B., Penuelas, J., Botella, C., Hollinger, G., & Saint-Girons, G. Heteroepitaxy of $SrTiO_3$ thin films on Si (001) using different growth strategies: Toward substratelike qualitya). *J. Vac. Sci. Technol. B.* **29** (4), 041207 (2011).
18. Yu, Z., *et al.* Advances in heteroepitaxy of oxides on silicon. *Thin Solid Films.* **462-463**, 51-56 (2004).
19. Yu, Z., *et al.* Epitaxial oxide thin films on Si (001). *J. Vac. Sci. Technol. B.* **18** (4), 2139-2145 (2000).
20. Demkov, A. A., & Zhang, X. Theory of the Sr-induced reconstruction of the Si (001) surface. *J. Appl. Phys.* **103** (10), 103710 (2008).
21. Zhang, X., *et al.* Atomic and electronic structure of the $Si/SrTiO_3$ interface. *Phys. Rev. B.* **68** (12), 125323 (2003).
22. Ashman, C. R., Först, C. J., Schwarz, K., & Blöchl, P. E. First-principles calculations of strontium on Si(001). *Phys. Rev. B.* **69** (7), 075309 (2004).
23. Kamata, Y. High-k/Ge MOSFETs for future nanoelectronics. *Mater. Today.* **11** (1-2), 30-38 (2008).
24. Fischetti, M. V., & Laux, S. E. Band structure, deformation potentials, and carrier mobility in strained Si, Ge, and SiGe alloys. *J. Appl. Phys.* **80** (4), 2234-2252 (1996).
25. Liang, Y., Gan, S., Wei, Y., & Gregory, R. Effect of Sr adsorption on stability of and epitaxial $SrTiO_3$ growth on Si(001) surface. *Phys. Status Solidi B.* **243** (9), 2098-2104 (2006).
26. McDaniel, M. D., *et al.* A Chemical Route to Monolithic Integration of Crystalline Oxides on Semiconductors. *Adv. Mater. Interfaces.* **1** (8), (2014).
27. Leskelä, M., & Ritala, M. Atomic layer deposition (ALD): from precursors to thin film structures. *Thin Solid Films.* **409** (1), 138-146 (2002).
28. George, S. M. Atomic Layer Deposition: An Overview. *Chem. Rev.* **110** (1), 111-131 (2010).
29. McDaniel, M. D., Posadas, A., Wang, T., Demkov, A. A., & Ekerdt, J. G. Growth and characterization of epitaxial anatase $TiO_2(001)$ on $SrTiO_3$-buffered Si(001) using atomic layer deposition. *Thin Solid Films.* **520** (21), 6525-6530 (2012).
30. McDaniel, M. D., *et al.* Growth of epitaxial oxides on silicon using atomic layer deposition: Crystallization and annealing of TiO_2 on $SrTiO_3$-buffered Si(001). *J. Vac. Sci. Technol. B.* **30** (4), 04E111 (2012).
31. McDaniel, M. D., *et al.* Epitaxial strontium titanate films grown by atomic layer deposition on $SrTiO_3$-buffered Si(001) substrates. *J. Vac. Sci. Technol. A.* **31** (1), 01A136 (2013).

32. Ngo, T. Q., *et al.* Epitaxial growth of $LaAlO_3$ on $SrTiO_3$-buffered Si (001) substrates by atomic layer deposition. *J. Cryst. Growth.* **363**, 150-157 (2013).
33. Ngo, T. Q., *et al.* Epitaxial c-axis oriented $BaTiO_3$ thin films on $SrTiO_3$-buffered Si(001) by atomic layer deposition. *Appl. Phys. Lett.* **104** (8), 082910 (2014).
34. McDaniel, M. D., *et al.* Incorporation of La in epitaxial $SrTiO_3$ thin films grown by atomic layer deposition on $SrTiO_3$-buffered Si (001) substrates. *J. Appl. Phys.* **115** (22), 224108 (2014).
35. McDaniel, M. D., *et al.* Atomic layer deposition of crystalline $SrHfO_3$ directly on Ge (001) for high-k dielectric applications. *J. Appl. Phys.* **117** (5), 054101 (2015).
36. Ngo, T. Q., *et al. Integration of Ferroelectric Perovskites on Ge(001) by ALD: A Case Study of $BaTiO_3$.* at <http://www2.avs.org/symposium2014/Papers/Paper_EM+MI+NS-MoM11.html> (2014).
37. Jahangir-Moghadam, M., *et al.* Band-Gap Engineering at a Semiconductor-Crystalline Oxide Interface. *Adv. Mater. Interfaces.* **2** (4), (2015).
38. Posadas, A., *et al.* Epitaxial integration of ferromagnetic correlated oxide $LaCoO_3$ with Si (100). *Appl. Phys. Lett.* **98** (5), 053104 (2011).
39. Ponath, P., Posadas, A. B., Hatch, R. C., & Demkov, A. A. Preparation of a clean Ge(001) surface using oxygen plasma cleaning. *J. Vac. Sci. Technol. B.* **31** (3), 031201 (2013).
40. Braun, W. *Applied RHEED: Reflection High-Energy Electron Diffraction During Crystal Growth.* Springer Science & Business Media (1999).
41. Moulder, J. F., Stickle, W. F., Sobol, P. E., & Bomben, K. E. *Handbook of X-ray Photoelectron Spectroscopy.* Perkin-Elmer Corporation: Eden Prairie, MN (1992).
42. Vehkamäki, M., Hatanpää, T., Hänninen, T., Ritala, M., & Leskelä, M. Growth of $SrTiO_3$ and $BaTiO_3$ thin films by atomic layer deposition. *Electrochem. Solid-State Lett.* **2** (10), 504-506 (1999).
43. Vehkamäki, M., *et al.* Atomic Layer Deposition of $SrTiO_3$ Thin Films from a Novel Strontium Precursor-Strontium-bis(tri-isopropyl cyclopentadienyl). *Chem. Vap. Depos.* **7** (2), 75-80 (2001).
44. Ritala, M., Leskelä, M., Niinisto, L., & Haussalo, P. Titanium isopropoxide as a precursor in atomic layer epitaxy of titanium dioxide thin films. *Chem. Mater.* **5** (8), 1174-1181 (1993).
45. Aarik, J., Aidla, A., Uustare, T., Ritala, M., & Leskelä, M. Titanium isopropoxide as a precursor for atomic layer deposition: characterization of titanium dioxide growth process. *Appl. Surf. Sci.* **161** (3-4), 385-395 (2000).
46. Premkumar, P. A., Delabie, A., Rodriguez, L. N. J., Moussa, A., & Adelmann, C. Roughness evolution during the atomic layer deposition of metal oxides. *J. Vac. Sci. Technol. A.* **31** (6), 061501 (2013).

